SAND2016-11182C

Energy Based Representation of 6-DOF Shaker Shock Low-Cycle Fatigue Tests

Carl Sisemore, Vit Babuska, Jason Booher
Sandia National Laboratories, PO Box 5800, Albuquerque, NM 87185-0840

ABSTRACT

Materials subject to cyclic loading have been studied extensively and experimentally determined comparisons of stress to number of cycles are used to estimate fatigue life under various loading scenarios. Fatigue data are traditionally presented in the form of S-N curves. Normally, S-N data are derived from cyclic loading but the S-N results are also applicable to random vibration loading and, to some extent, shock. This paper presents an alternate presentation of fatigue data in terms of input energy and number of cycles to failure. In conjunction with this study, a series of shock tests was conducted on 3D printed cantilever beams using a 6-DOF shaker table. All of the beams were tested to failure at shock levels in the low-cycle fatigue regime. From these data, a nominal fatigue curve in terms of input energy and number of shocks to failure was generated and compared with the theoretical developments.

INTRODUCTION

Energy response spectra, along with the shock response spectrum (SRS), are both valid methods for quantifying the severity of single mechanical shock events. The SRS was introduced in the 1930's and is currently the standard method for describing mechanical shock events. Energy spectra methods for the analysis of mechanical shock are nearly as old as the SRS, being introduced in the 1950's. The seismic and civil engineering community has long used the energy methods, including energy response spectra, for describing damage potential to structures from earthquakes. Energy response spectra are generally analogous to the SRS but are based on other quantities such as potential, kinetic, and total energy.

In the seismic community the shock loading is typically a single earthquake event and the structure either passes or fails accordingly. However, many shock scenarios in other disciplines are based on events related to transportation: ground or air transport. As such, the number of shock events could be quite high as the component of interest is transported from one location to another. This leads to the concept of low or high-cycle fatigue shock loading. SRS methods are only applicable to single shocks in which the failure mechanism is an overstress. In contrast, energy quantities seem better suited to capturing the cumulative effects of multiple shocks.

The purpose of this investigation was first to determine how 6-DOF shock testing related back to single degree-of-freedom shock testing. The 6-DOF testing used herein applied shocks simultaneously in all three translational directions as well as three rotational shocks. The second goal of this investigation was to better understand how energy quantities apply to repetitive shock events and to develop a theoretical framework for their application. Do energy metrics follow a similar framework as more traditional fatigue life estimation methods?

This paper describes the results of a series of 6-DOF shaker shock tests performed on ABS plastic cantilever beams manufactured with a 3D printer. Over three thousand 6-DOF shocks were applied to 68 different cantilever beams during the course of this study. The general test approach was to test several beams simultaneously at a level below that known to cause failure with one shock and repeat that test until all beams failed. The test was then repeated with a new set of beams and a different low-level shock input. The test specifics, data processing, and results are described in this paper along with an appropriate failure theory based on input energy.

BASQUIN'S EQUATION FOR SHOCK

Endurance of materials subject to cyclic loading has been extensively studied since the 1800's. The endurance life or fatigue life, defined as the number of cycles to failure or the ability of a machine part to resist fatigue, is dependent on the developed stress in the part. The data from these tests characterizing the endurance of the material are displayed as S-N curves. The S-

N curve in the high-cycle fatigue region can be represented analytically. The most popular representation is the Basquin relation:

$$NS^b = C. \tag{1}$$

In the above equation, N is the number of cycles to failure, S is the cyclical stress amplitude, b is the fatigue strength coefficient, and C is an empirically determined constant. The fatigue strength coefficient is determined from S-N data where $-1/b$ is the slope of the S-N line in log-log space.

Basquin's equation is a model based on test data. Fatigue strength coefficients typically range from 3 – 25 with the most common values falling between 3 and 10. Lalanne [1] has compiled typical fatigue strength coefficient values for a variety of materials (aluminum, steel, solder) and components (resistors, capacitors, circuit boards, and other complex electronic items) measured from numerous tests. The spacecraft community has settled on a fatigue strength coefficient of 4.0 for electronic and electrical equipment, 6.4 for load carrying structures under sinusoidal vibration, and 8.0 for load carrying structures under random vibration [2,3].

Basquin's equation is popular and has been used for more than 60 years for several reasons: it fits measured data well; it is consistent with fracture mechanics models; and it can be adjusted to account for factors such as surface finish, corrosion, stress concentration factors, stress ratios, and others as needed.

It has been postulated previously that a power law relationship like Basquin's equation applies to shock environments and energy spectra comparisons [4]. In this context, the Basquin equation would be defined in terms of some energy quantity and number of cycles to failures.

INPUT ENERGY AND FATIGUE LIFE

In the energy framework, fatigue life is a function of the input energy, which can be calculated for any dynamic system as:

$$E_I = \int_{t=0}^{t=T} \boldsymbol{p}(t) \cdot \dot{\boldsymbol{x}}(t) dt \tag{2}$$

where $\boldsymbol{p}(t)$ is an external load vector and $\dot{\boldsymbol{x}}(t)$ is the response velocity vector. Note that input energy includes a response term. This means that the input energy can vary across a structure depending on the response location. In the subsequent development, there is an implicit assumption that the input energy is calculated for the component of interest.

The S-N plot is the experimentally determined relationship between zero mean, constant cyclic stress amplitude and number of cycles to failure. To create a similar E_I-N curve from an S-N curve, consider the case of constant amplitude cyclic loading. In this case $p(t) = A\sin(\Omega t)$, and any environment is characterized by $[p(t),T]$ or $[A,\Omega,T]$. For steady state cyclic loading, the input energy can be written as:

$$E_I = \int_{t=0}^{N/\Omega} \boldsymbol{p}(t)\,\dot{\boldsymbol{x}}(t) dt = N \int_{t=0}^{1/\Omega} \boldsymbol{p}(t)\dot{\boldsymbol{x}}(t) dt = N\overline{E_I} \tag{3}$$

where N is the number of cycles and $\overline{E_I}$ is the input energy per cycle.

Input energy per cycle has another interpretation—as the energy dissipated per cycle. If a dissipative system starts and ends at rest, with no permanent deformation, the total input energy is equal to the total dissipated energy, $E_I = E_D$. So it follows by extension that $\overline{E}_I = \overline{E}_D$.

This relationship can be used to generate the E_I-N curve. Damping energy is proportional to the square of the stress amplitude, S, in linear dynamical systems with viscous damping [5]. Thus, it is apparent that

$$\bar{E}_D \propto S^2 \tag{4}$$

Substituting Equation 4 into Equation 1 implies that dissipated energy also follows a power law relationship with the number of cycles.

$$N\bar{E}_D^{\frac{b}{2}} = C_D \tag{5}$$

where C_D is an empirically determined constant, not necessarily the same as C from Equation 1. Rearranging this equation gives:

$$\bar{E}_I = \bar{E}_D = C_D^{\frac{2}{b}} N^{-\frac{2}{b}} \tag{6}$$

This form of the equation is consistent with the way S-N curves are shown graphically whereas the original form of Equation 1 is consistent with fracture mechanics models. The slope of the S-N curve is $-1/b$, so the slope of a corresponding $\bar{E}_I$-N curve is twice the slope of the S-N curve. Thus, in terms of total input energy or total dissipated energy, Equation 6 becomes

$$E_I = E_D = N\bar{E}_I = C_D^{\frac{2}{b}} N^{\left(1-\frac{2}{b}\right)} \tag{7}$$

While damping energy is approximately proportional to the square of stress amplitude as shown in Equation 4, Dowling provides a more realistic relationship between stress and damping energy as a non-linear function of stress amplitude [5]. For metals, this relationship is given as

$$\bar{E}_D \propto S^{\beta} \begin{cases} \beta \sim 2.4, S < 0.8S_{yield} \\ \beta \sim 8\ , S \geq 0.8S_{yield} \end{cases} \tag{8}$$

Thus, the more general form of Equation 6 is:

$$\bar{E}_I = C_D^{\frac{\beta}{b}} N^{-\frac{\beta}{b}} \tag{9}$$

For high-cycle fatigue, generally, $S < 0.8S_{yield}$ suggesting that $\beta = 2.4$ is appropriate and slightly more conservative than $\beta = 2$. A common average value for the fatigue strength coefficient for general structural members is $b = 6.67$ which is consistent with References 2 and 3. The slope of the S-N curve is then $-1/b \cong -0.15$, so a typical slope of the $\bar{E}_I$-N curve is about -0.36 and the slope of the corresponding E_I-N curve would be 0.64.

The main implication of the similarity between the S-N curve and the $\bar{E}_I$-N curve is that all of the machinery developed for high-cycle fatigue analysis is applicable when the quantity of interest is input energy instead of stress—specifically Miner's rule.

TEST ARTICLE DESCRIPTION

The test article of interest in this study are ABS plastic 3D printed cantilever beams printed by the Sandia National Laboratories Additive Manufacturing group. The beams were printed with crosswise rastering. Crosswise raster printing produces brittle beams with inhomogeneous material properties. Figure 1 shows the brittle nature of the beams in stress strain curves measured during static testing of crosswise raster printed cylindrical coupons. The elastic properties were measured at slow strain rates. At higher strain rates, typical of shock loading, the material may be more brittle. Figure 2 is a micrograph of a cross section of one of the coupons. The printing orientation is clearly visible as is the inhomogeneity of the material.

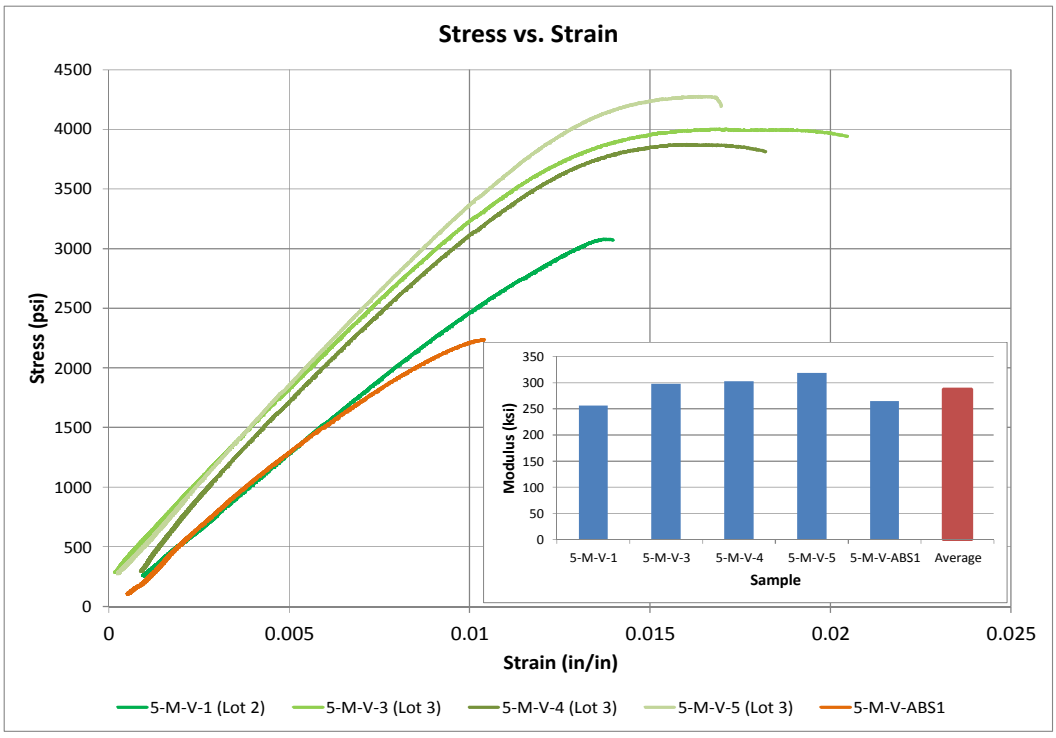

Figure 1. Modulus of ABS Plastic Beams

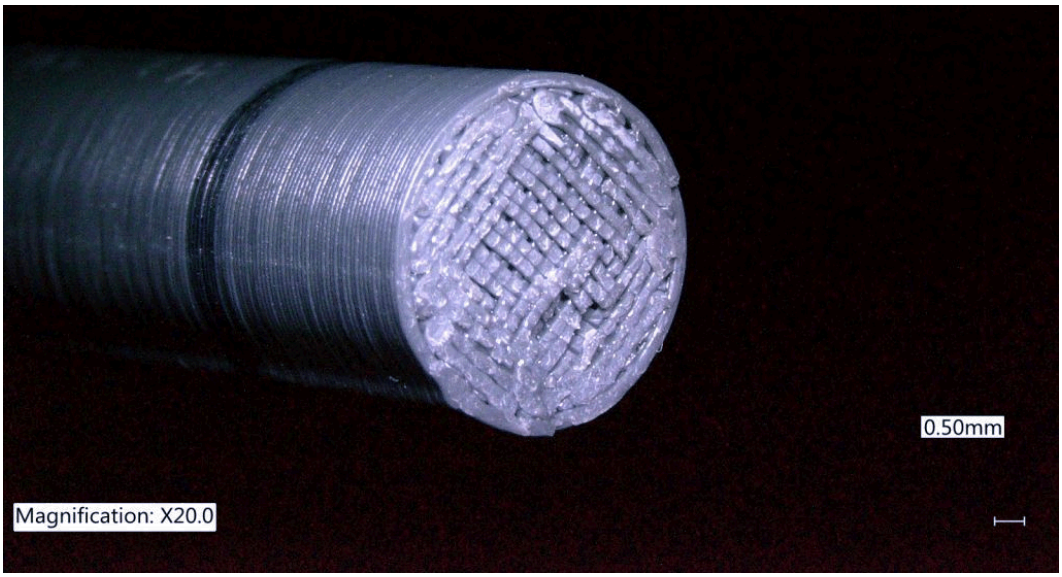

Figure 2. Micrograph of ABS Beam Cross-section

The S-N and E_I-N relationships were derived using characteristics of high-cycle fatigue behavior. The source of high cycle fatigue failure is usually a flaw such as a microcrack or void that is irritated by even low levels of strain so that a crack initiates. Low cycle fatigue is usually characterized by cyclic loading that induces plastic deformation. The slope of the S-N curve in this region is smaller than the slope in the high cycle region. Once the yield stress is exceeded, strain based fatigue models must be used because stress and strain are no longer linearly related, but an S-N curve can be approximated using empirically deduced models (e.g., Coffin model). However, brittle materials, by their very nature, do not tolerate large strains well. Inhomogeneous materials such as the 3D printed plastic have intrinsic microstructural (and macrostructural)

failure initiation mechanisms. Therefore, a high-cycle fatigue model may apply to the 3D printed beams in that there is no low-cycle fatigue region because they are brittle; i.e., the S-N curve has a constant slope down to a very low number of cycles. Furthermore, the macroscopic flaws are analogous to the microscopic flaws in metals, so the slope of the S-N curve of the 3D printed beams curve may be in-family with typical published values.

6-DOF SHOCK TESTING OVERVIEW

For the experimental portion of this study, the 68 ABS plastic 3D printed cantilever beams were tested on the Sandia National Laboratories large 6-DOF shaker table. A photograph of the test setup is shown in Figure 3. The tests were conducted in 17 sets with four beams per tests. The first test sets were performed by incrementally stepping up the input shock load until all four beams failed. Typically, most beams failed after a few shocks. The second round of testing was performed to quantify fatigue failures for cantilever beams of the same design. For the fatigue tests, a test level less than the failure level was selected and that test was repeated until all beams failed. The test was then repeated with new beams and a different shock input level.

Figure 4 shows a close-up photograph of a set of three inch long cantilever beams installed in the test fixture. Testing was performed on both three inch and five inch long cantilever beams in this study. Also shown in this figure are a set of steel clamp-on collar weights and the stress concentration notch near the cantilever beam's base.

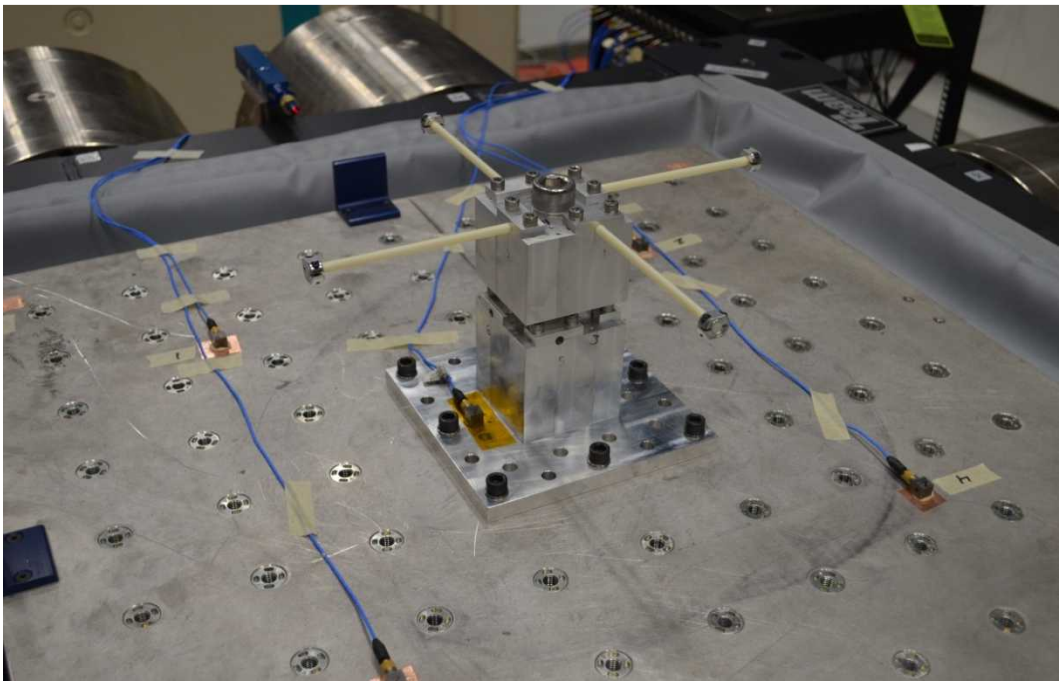

Figure 3. Cantilever Beam Test Fixture and Test Specimen Installed on 6-DOF Shaker Table

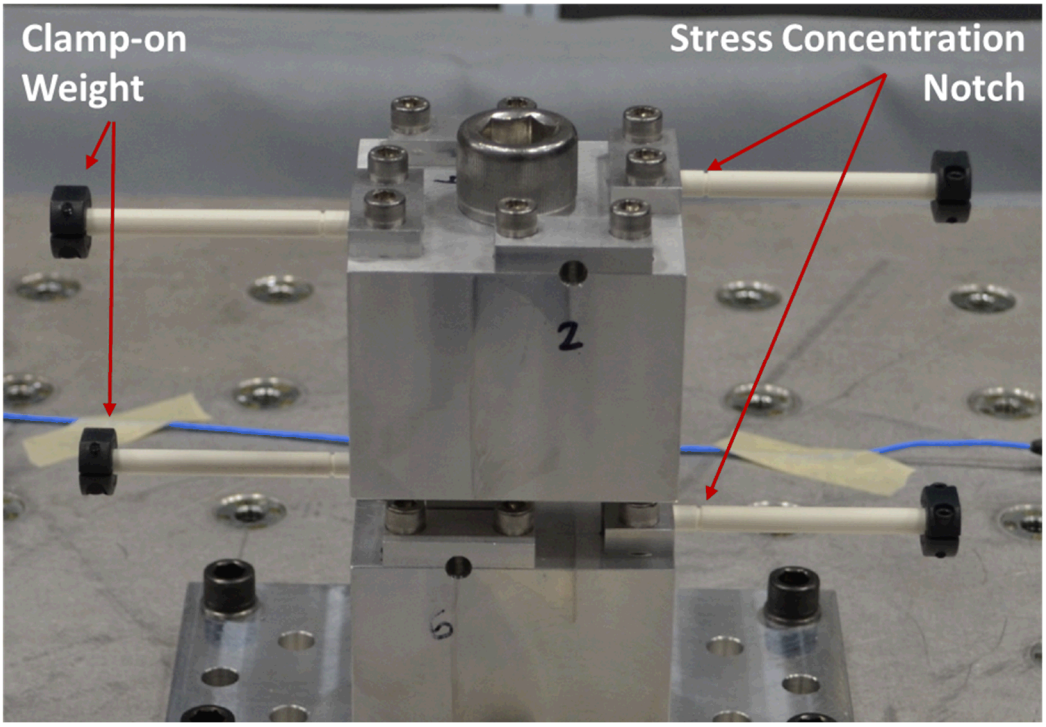

Figure 4. Photograph of the Test Fixture with 3-D Printed Cantilever Beams Installed Showing the Clamp-on Collar Weights and the Stress Concentration Notch

A total of 3,424 shocks were performed on the 6-DOF shaker table divided among the 17 test series. All failures were brittle failures by design due to the crosswise raster orientation of the 3D printed beams. It was noted that many beams developed obvious cracks prior to failure; however, the cracks were not always readily propagated through the cross-section. It appeared that some of the cracks caused the fundamental beam frequency to shift to a region outside of the shaker excitation frequency band, thus slowing crack growth significantly.

Instrumentation for these tests consisted of five tri-axial accelerometers, one mounted at the base of the upright beam fixture and the other four mounted near each of the four corners of the table as shown in Figure 3. These five measurements allowed for determination of the table translations and rotations.

Figure 5 shows a plot of a typical translational acceleration time history from a 6-DOF shock event. The acceleration shown here is the average table acceleration input in each direction. Figure 6 shows a similar plot of the typical rotational acceleration time histories from the same shaker shock event. The rotational acceleration time histories had to be derived from the tri-axial accelerometers at the table corners. For this analysis it was assumed that the table's center of rotation was coincident with the table's geometric center. The resulting calculations indicated that there was a slight difference between the table's geometric center and the center of rotation. The difference was very small and thus it was ignored for this analysis, consistent with previous researchers [6].

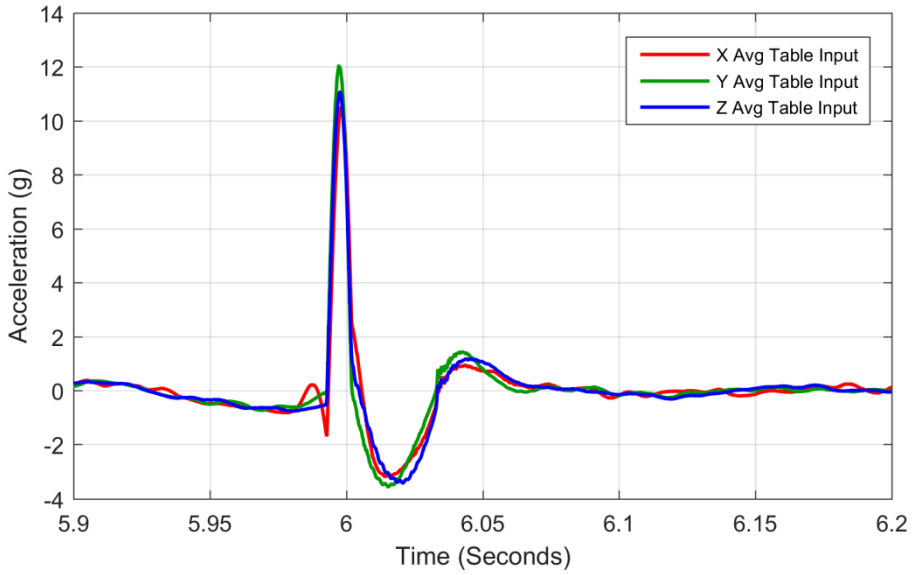

Figure 5. Typical Translational Acceleration Profile from 6-DOF Shaker Shock Tests

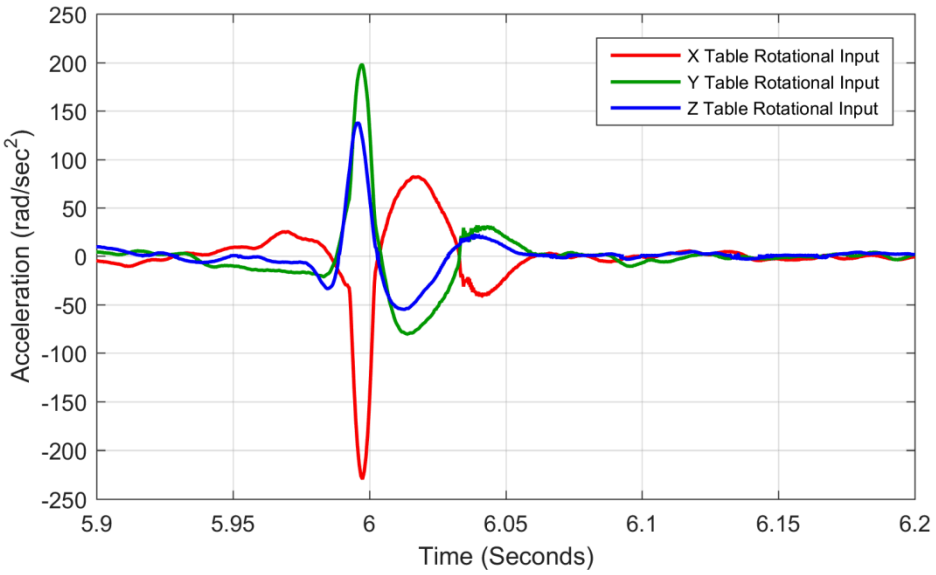

Figure 6. Typical Rotational Acceleration Profile from 6-Dof Shaker Shock Tests

DERIVATION OF 6-DOF COMPOSITE ENERGY SPECTRA

Calculating an energy spectrum from a single translational input is a relatively simple task. However, to evaluate the failure results from 6-DOF testing it is necessary to extend the energy spectrum concept to account for simultaneous rotational and translational shocks. This extension is necessary to generate comparisons with analytical single-axis failure predictions and single-axis test to failure results.

Since the energy spectrum formulations all have a component of velocity, as seen in Equation 2, and there is a direct relationship between velocity, or pseudo-velocity SRS (PVSRS) and stress, a composite 6-DOF SRS based on PVSRS is appropriate. The details of this 6-DOF composite SRS derivation are presented in [7] and are summarized here. Figure 7

shows a hypothetical cantilever beam oriented with respect to the 6-DOF coordinate system. Here, the x-axis is oriented parallel to the cantilever beam's long axis but offset by a distance h. This coordinate system corresponds well with the actual 6-DOF shaker coordinate system where it is assumed that the table's center of rotation is at the geometric center of the table face but the part under test will of necessity be mounted some distance above the table face.

The concept of a composite pseudo-velocity SRS is needed to relate the three translational SRS and three rotational SRS from the 6-DOF shock input to failure of the test article. It is obvious that failure should not be equal to any single axis response individually but to the combination of all inputs loading the structure. Each of the six shocks induces normal stresses in the structure—bending stress from transverse shocks and axial stress from axial shocks. Figure 7 shows the coordinate system assumed for the composite SRS calculations with axial shocks occurring along the x-axis and transverse shocks occurring in the y- or z-axes.

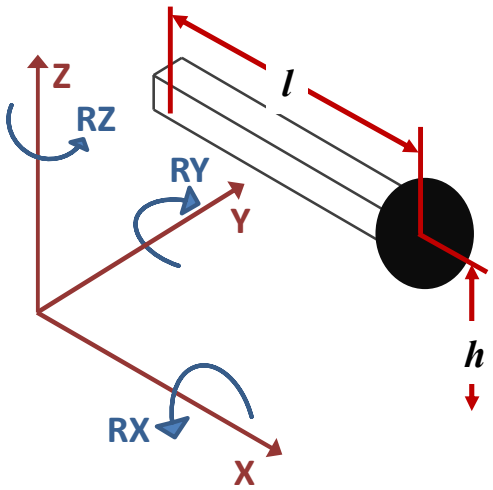

Figure 7. Cantilever Beam and Coordinate System for 6-DOF Tests

There are several methodologies for combining multi-axis stress such as the von Mises or maximum distortional energy theory, maximum principal stress theory, or the Tresca or maximum shear stress theory for example. However, in this case, the derivation is performed in terms of pseudo-velocity SRS since actual stress was not measured. In the derivation presented in [7], an effective axial and bending PVSRS for each of the three directions was presented as:

$$PV_{xeff} = PV_x$$

$$PV_{yeff} = PV_y + PV_{rz}l + PV_{rx}h \tag{10}$$

$$PV_{zeff} = PV_z + PV_{ry}l$$

where l and h are the distances shown in Figure 7. Equation 10 reduces the original six shock relations to three and is the first step in creating a single, composite spectrum. It is based on the kinematic velocity equation:

$$V = v_T + \omega xr \tag{11}$$

where V is the total velocity, v_T is the translational velocity ω is the rotational velocity. For the cantilever beam shown in Figure 7, a composite pseudo-velocity SRS from the 6-DOF shock input is given by the relationship:

$$PV_{composite} = \frac{r}{4l}PV_{xeff} + \sqrt{(PV_{yeff})^2 + (PV_{zeff})^2}. \tag{12}$$

This relationship was derived and demonstrated by testing documented in [7] for the cantilever beams tested here. From the pseudo-velocity, a composite expression for the absorbed energy spectrum can be directly calculated as given by Hudson [8] from:

$$E_{Am} = \frac{1}{2} PV^2. \tag{13}$$

Thus, it is apparent that the absorbed energy can also be calculated by:

$$E_{Am} = \frac{1}{2} PV^2_{composite} = \frac{1}{2}\left[\frac{r}{4l} PV_{xeff} + \sqrt{\left(PV_{yeff}\right)^2 + \left(PV_{zeff}\right)^2}\right]^2. \tag{14}$$

It has been shown previously that a similar relationship exists for input energy [7]. Input energy can be calculated for each of the six shocks, converted to an analogous velocity spectrum using the inverse of Equation 13 and combined in a similar fashion as Equation 14 to yield a composite input energy spectrum. It is this resulting composite input energy spectrum that is used to derive the low-cycle fatigue results from the testing described here.

6-DOF SHOCK TEST RESULTS

The 6-DOF shock tests applied a similar shock load simultaneously in all six degrees of freedom as shown previously. For the initial tests, the shock loads were applied once and then incrementally increased for subsequent shocks until all beams failed. Most beams in a set failed at the same shock level or at consecutive shock levels indicating that the failure levels were reasonably consistent for parts of the same design. Following the initial testing, low-cycle fatigue testing was performed by selecting a shock test level less than the determined failure load and repeating that shock until all beams in the set failed. A different shock input level was then selected and the test repeated. From the data collected, a composite input energy spectrum was calculated for each shock as detailed previously and the sum of the input energy from all shocks experienced by a given cantilever beam was calculated. Figure 8 shows a plot of the total input energy compared to the number of shocks to failure from the elliptic cantilever beam tests. The slope of the least squares fit straight line through the data is 0.65 which is nearly identical to the predicted slope of 0.64 for common structural materials. While this is very interesting that the measured slope and the theoretical slope are very close, it may be a coincidence since the theoretical slope is derived from a nominal value for common structural materials. However, it is significant that the slope is in family with structural materials and not substantially different from the basic theory.

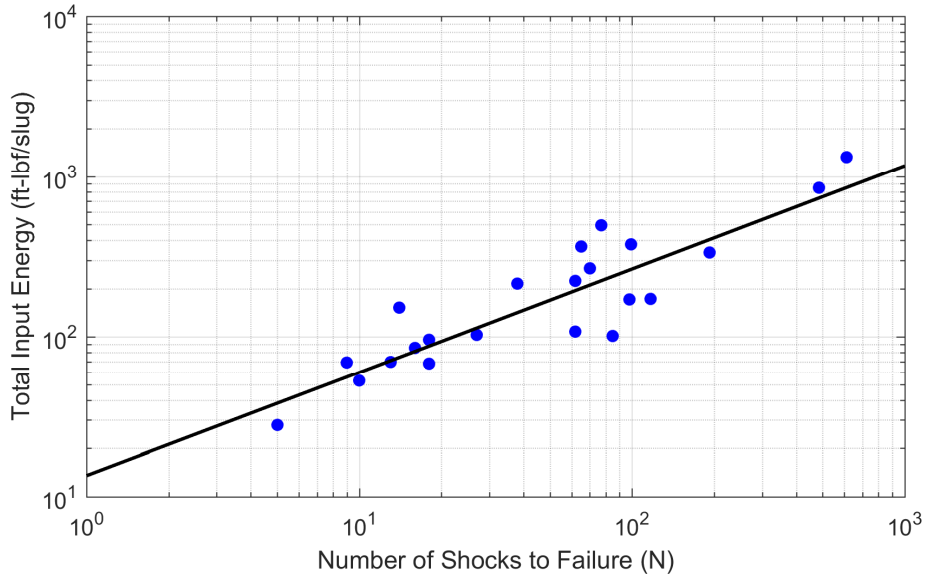

Figure 8. Plot of Number of Shocks to Failure versus Total Input Energy from 6-DOF Cantilever Beam Tests

Figure 9 shows a plot of the same elliptic beam 6-DOF fatigue test data, this time formatted to show the number of shocks to failure compared to the average input energy per shock. Since all of the shock events for a single test series were nominally the same, the input energy from all the shocks was averaged. The slope of the least squares fit straight line through the data

is −0.35 which is again nearly equal to the predicted slope of −0.36 for common structural materials. Here again, the significance is not in the closeness of the result exactly but rather that the result is in family with general structural materials which confirms that the fatigue relationships derived here for input energy are similar to the more common S-N curve results with similar Basquin equation exponents.

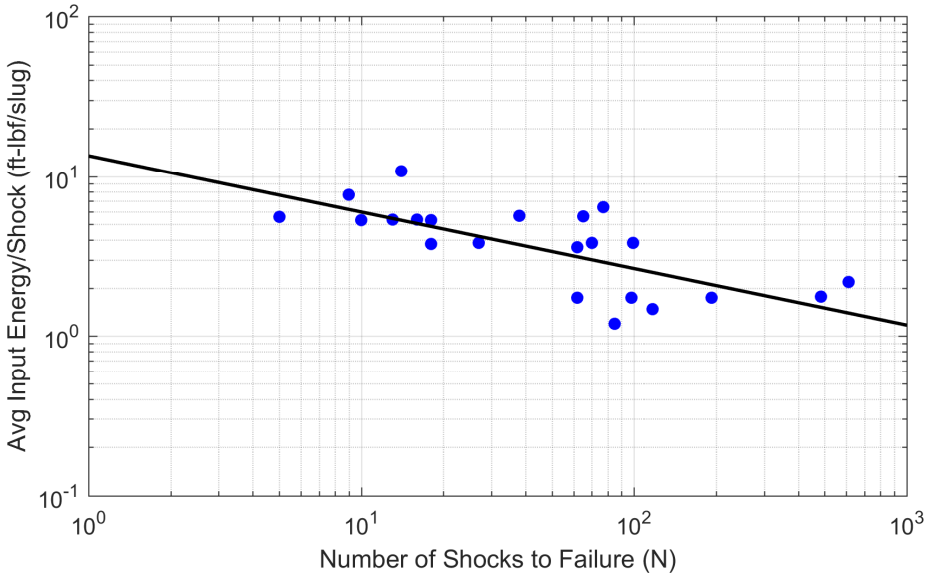

Figure 9. Plot of Number of Shocks to Failure versus Average Input Energy from 6-DOF Cantilever Beam Tests

CONCLUSIONS

A power-law relationship between input energy and number of cycles was derived for high and low-cycle fatigue. This relationship was extended to low-cycle fatigue from the application of multiple low level shocks.

The equation, like the traditional S-N relationship, depends on experimental data to define empirical coefficients. Experiments with cantilever beams on a 6-DOF shaker were performed to estimate the coefficients for ABS plastic. The 6-DOF shaker introduced a multi-axial stress state in the beams and a technique for accounting for the complex excitation was developed and applied to the test data.

The empirically determined coefficients were in family with those determined for most metals and general structural materials.

ACKNOWLEDGEMENT

Sandia National Laboratories is a multi-mission laboratory managed and operated by Sandia Corporation, a wholly owned subsidiary of Lockheed Martin Corporation, for the U.S. Department of Energy's National Nuclear Security Administration under contract DE-AC04-94AL85000.

REFERENCES

1. Lalanne, C., *Fatigue Damage, Mechanical Vibration and Shock Analysis, 3rd Edition,* Vol 4, John Wiley & Sons, New Jersey, 2014.
2. NASA Technical Handbook, *Dynamic Environmental Criteria*, NASA-HDBK-7005, National Aeronautics and Space Administration, 13 March 2001.

3. SMC Standard SMC-S-16, *Test Requirements for Launch, Upper Stage and Space Vehicles*¸13 June 2008, Section 10.2.2, page 109.
4. Babuška, V., Sisemore, C., and Booher, J., "Energy Based Representations of Mechanical Shock for Failure Characterization," Proceedings of the AIAA SciTech 2016 Conference, San Diego, California, January 2016.
5. Dowling, N. E., *Mechanical Behavior of Materials, Engineering Methods for Deformation, Fracture, and Fatigue, 3rd Edition*, Pearson , Prentice Hall, New Jersey, 2007, page 827-832.
6. Smallwood, D. O. and Gregory, D., "Evaluation of a Six-DOF Electrodynamic Shaker System," Proceedings of the 79th Shock and Vibration Symposium, Orlando, Florida, October 2008.
7. Sisemore, C., Babuška, V., and Booher, J., "6-DOF Mechanical Shock Failure Predictions of a Cantilever Structure Using Energy Response Spectra Methods," Proceedings of the 87th Shock and Vibration Symposium, New Orleans, Louisiana, October 2016.
8. Hudson, D. E., "Response Spectrum Techniques in Engineering Seismology," *Proceedings of the World Conference on Earthquake Engineering*¸ Berkeley, California, 1956, pp. 4.1–4.12.